UCSF
UC San Francisco Previously Published Works

Title

Selective Ablation of Tumor Suppressors in Parafollicular C Cells Elicits Medullary Thyroid Carcinoma*

Permalink

https://escholarship.org/uc/item/7rm474mf

Journal

Journal of Biological Chemistry, 292(9)

ISSN

0021-9258

Authors

Song, Hai
Lin, Chuwen
Yao, Erica
et al.

Publication Date

2017-03-01

DOI

10.1074/jbc.m116.765727

Copyright Information

This work is made available under the terms of a Creative Commons Attribution License, available at https://creativecommons.org/licenses/by/4.0/

Peer reviewed

eScholarship.org Powered by the California Digital Library
University of California

THE JOURNAL OF BIOLOGICAL CHEMISTRY VOL. 292, NO. 9, pp. 3888–3899, March 3, 2017
© 2017 by The American Society for Biochemistry and Molecular Biology, Inc. Published in the U.S.A.

Selective Ablation of Tumor Suppressors in Parafollicular C Cells Elicits Medullary Thyroid Carcinoma*

Received for publication, November 4, 2016, and in revised form, January 23, 2017 Published, JBC Papers in Press, January 24, 2017, DOI 10.1074/jbc.M116.765727

Hai Song[‡§], Chuwen Lin[§], Erica Yao[§], Kuan Zhang[§], Xiaoling Li[‡], Qingzhe Wu[‡], and Pao-Tien Chuang[§1]

From the [‡]Life Sciences Institute and Innovation Center for Cell Signaling Network, Zhejiang University, Hangzhou 310058, China and the [§]Cardiovascular Research Institute, University of California, San Francisco, California 94158

Edited by Xiao-Fan Wang

Among the four different types of thyroid cancer, treatment of medullary thyroid carcinoma poses a major challenge because of its propensity of early metastasis. To further investigate the molecular mechanisms of medullary thyroid carcinoma and discover candidates for targeted therapies, we developed a new mouse model of medullary thyroid carcinoma based on our *CGRP*^{CreER} mouse line. This system enables gene manipulation in parafollicular C cells in the thyroid, the purported cells of origin of medullary thyroid carcinoma. Selective inactivation of tumor suppressors, such as *p53*, *Rb*, and *Pten*, in mature parafollicular C cells via an inducible Cre recombinase from *CGRP*^{CreER} led to development of murine medullary thyroid carcinoma. Loss of *Pten* accelerated *p53*/*Rb*-induced medullary thyroid carcinoma, indicating interactions between pathways controlled by tumor suppressors. Moreover, labeling differentiated parafollicular C cells by *CGRP*^{CreER} allows us to follow their fate during malignant transformation to medullary thyroid tumor. Our findings support a model in which mutational events in differentiated parafollicular C cells result in medullary thyroid carcinoma. Through expression analysis including RNA-Seq, we uncovered major signaling pathways and networks that are perturbed following the removal of tumor suppressors. Taken together, these studies not only increase our molecular understanding of medullary thyroid carcinoma but also offer new candidates for designing targeted therapies or other treatment modalities.

Thyroid carcinoma represents the most common endocrine malignancy (1). Medullary thyroid carcinoma (MTC)[2] comprises ~5% of thyroid cancer (2). Compared with the more common papillary and follicular thyroid cancers, medullary thyroid carcinoma is prone to early metastasis to lymph nodes. Consequently, the survival rate of medullary thyroid carcinoma is comparatively lower. Treatment of these patients with advanced diseases poses a major challenge when surgical resection and use of radioiodine are no longer options (3–6). In fact, MTC accounts for more than 14% of thyroid cancer-related deaths. Uncovering new genes and pathways required for the development or survival of medullary thyroid carcinoma (7, 8) is critical to inventing novel targeted therapies or other options for treating these patients (9, 10).

Approximately 20% of medullary thyroid carcinomas are associated with inherited multiple endocrine neoplasia type 2 endocrine syndromes, and the remaining 80% are sporadic (11). Most hereditary medullary thyroid carcinomas harbor mutations in RET (rearranged during transfection) (12, 13), a receptor tyrosine kinase, which signals through the RAS-MAPK and PI3K-AKT pathways (14). Similarly, *RET* mutations have been identified in a significant fraction (40–50%) of sporadic medullary thyroid carcinoma (15).

In addition to *RET*, genetic analysis of mice deficient in tumor suppressors revealed a role for these genes in medullary thyroid carcinoma development. For instance, *Rb*-deficient mice developed medullary thyroid carcinoma. Conditional inactivation of *Rb* using *Villin-Cre* also induced highly aggressive medullary thyroid carcinoma in mice (16). Moreover, conditional inactivation of *Rb* throughout gestation via a surfactant protein C-rtTA/tetO-Cre system resulted in medullary thyroid tumors caused by Cre induction in a subset of thyroid cells (17). Loss of *p53* in addition to *Rb* led to rapid tumor progression in this model (17). Interestingly, medullary thyroid carcinoma from *Rb*/*p53* heterozygous mice carried somatic cysteine mutations in RET, which were observed in human medullary thyroid carcinoma (18). Elucidating the molecular interactions between mutant RET and other oncogenes/tumor suppressors during medullary thyroid carcinoma development will further our understanding of how signaling pathways control tumor initiation, progression, and metastasis. This approach when complemented by genomic and expression analysis of medullary thyroid carcinoma or cell-based screens would offer new candidates for targeted therapies in patients with metastatic medullary thyroid carcinoma.

Medullary thyroid carcinoma is generally believed to originate from parafollicular C cells that are interspersed in the interstitial space between thyroid follicles (19). By contrast, the other three types of thyroid cancers (papillary, follicular, and

* This work was supported by National Natural Science Foundation of China Grant 31471368 and Zhejiang Provincial Natural Science Foundation of China Grant LR16C120001 (to H. S.) and National Institutes of Health Grants U01 HL111054 and R01 HL115207 (to P.-T. C.). The authors declare that they have no conflicts of interest with the contents of this article. The content is solely the responsibility of the authors and does not necessarily represent the official views of the National Institutes of Health.

[1] To whom correspondence should be addressed: Cardiovascular Research Institute, University of California, San Francisco, 555 Mission Bay Blvd. S., San Francisco, CA 94158. Tel.: 415-514-0667; E-mail: pao-tien.chuang@ucsf.edu.

[2] The abbreviations used are: MTC, medullary thyroid carcinoma; CT, calcitonin; CGRP, calcitonin gene-related peptide; SYP, synaptophysin; TM, tamoxifen; DKO, double knock-out; TKO, triple knock-out; qPCR, quantitative PCR; IPA, Ingenuity Pathway Analysis; GPCR, G protein-coupled receptor; LXR, liver X receptor; RXR, retinoid X receptor.

anaplastic) are derived from the follicular epithelium. This conclusion is mainly derived from the observation that medullary thyroid tumor cells display immunohistological features characteristic of parafollicular C cells including secretion of neuropeptides such as calcitonin (CT), calcitonin gene-related peptide (CGRP), chromogranin A, and synaptophysin (SYP). Furthermore, transgenic overexpression of mutant forms of RET proteins, which are found in hereditary medullary thyroid carcinoma, using a 2-kb *CT*/*CGRP* promoter fragment led to medullary thyroid carcinoma in mice (20). In this setting, the *CT*/*CGRP* promoter fragment would drive mutant RET protein overexpression during thyroid development in embryogenesis and throughout adult life at a level significantly higher than that of endogenous Ret. Importantly, these transgenic mice recapitulate essential aspects of hereditary medullary thyroid carcinoma.

Although there is a consensus on the origin of medullary thyroid carcinoma, the nature of tumor-initiating cells and the early events of medullary thyroid carcinoma development are not fully understood. One approach to address these issues is to utilize the inducible Cre-lox system in mice to manipulate gene activity selectively in parafollicular C cells at physiological levels. This would permit production of mouse models of both hereditary and sporadic medullary thyroid carcinomas. The interactions between tumor suppressors during development of medullary thyroid carcinoma can be illuminated. In addition, this approach will provide insight into early stages of medullary thyroid carcinoma. These studies would complement published work on animal models of medullary thyroid tumors that largely rely on global, non-selective, or non-inducible gene activation/inactivation in the thyroid (21).

In this study, we utilized the $CGRP^{CreER}$ (22) and $Ascl1\text{-}(Mash1)^{CreER}$ (23) mouse strains that allowed us to control gene expression specifically in parafollicular C cells. By inactivating tumor suppressors in lineage-labeled parafollicular C cells, we revealed synergistic interactions between tumor suppressors during medullary thyroid carcinoma development. This system also demonstrated that medullary thyroid carcinoma can originate from differentiated parafollicular C cells. RNA-Seq analysis of murine medullary thyroid tumors uncovered pathways and networks perturbed in the absence of tumor suppressors. Selecting driver mutations from these studies will provide new candidates for targeted therapies or other treatment methods of medullary thyroid carcinoma.

Results

Inducible Expression of CreER from the Mouse Calca or Ascl1 Locus Confers Spatial and Temporal Control of Gene Expression in Parafollicular C Cells of the Thyroid Gland—To regulate gene activity in parafollicular C cells, we utilized the $CGRP^{CreER}$ mouse line that we previously reported (22). In this strain, CreER was introduced into the endogenous mouse *Calca* (calcitonin/calcitonin-related polypeptide, alpha) locus by gene targeting (24, 25). Transcripts from the *Calca* locus encode CT and CGRP because of tissue-specific alternative RNA splicing. $CGRP^{CreER}$ is selectively expressed in differentiated parafollicular C cells in the thyroid. CreER encodes a fusion protein of Cre recombinase and estrogen receptor, and CreER is active only when tamoxifen (TM) is present (26). In this system, tamoxifen administration to $CGRP^{CreER}$ mice provides an efficient way to control Cre activity in a temporally and spatially specific manner. For example, tamoxifen injection into adult $CGRP^{CreER}$ mice would confer exclusive Cre activation in parafollicular C cells after thyroid development is completed (Fig. 1*A*). When combined with the widely used Cre-lox system, $CGRP^{CreER}$ offers an essential tool to manipulate gene activity in parafollicular C cells to assess their role in medullary thyroid tumor development.

To test the efficiency and specificity of CreER expression in $CGRP^{CreER}$ mice, we bred $CGRP^{CreER}$ mice with $ROSA26^{mTmG}$ reporter mice (27) to generate mice carrying the genotype of $CGRP^{CreER/+}$; $ROSA26^{TmG/+}$. Cre activation upon tamoxifen administration resulted in eGFP expression from the $ROSA26^{mTmG}$ allele by removing sequences that block its expression (Fig. 1, *B–S*). Parafollicular C cells were identified using multiple markers including anti-CT, anti-SYP, and anti-ASCL1 (MASH1) (Fig. 1, *F*, *I*, *L*, and *O*). The specificity of CreER expression in parafollicular C cells was demonstrated by the observation that no eGFP expression was detected without TM injection (Fig. 1, *E–G*) and cells not expressing markers of parafollicular C cells were not labeled by eGFP in $CGRP^{CreER/+}$; $ROSA26^{mTmG/+}$ thyroid following tamoxifen treatment (Fig. 1, *H–P*). Follicular cells marked by NKX2.1 were not labeled by eGFP in $CGRP^{CreER/+}$; $ROSA26^{mTmG/+}$ thyroid, whereas parafollicular C cells expressed both NKX2.1 and eGFP (Fig. 1, *Q–S*). Depending on the dose and frequency of tamoxifen administration, ~90% of parafollicular C cells can be labeled by eGFP (Fig. 1, *H–P*), indicating efficient recombination in this cell type. No expression of eGFP was detected in parafollicular C cells in $ROSA26^{mTmG/+}$ mice under a similar condition. *R26R* reporter mice (28) gave identical results to $ROSA26^{mTmG/+}$ reporter mice. These findings indicate that CreER expression from $CGRP^{CreER}$ mice is specific and sufficient to permit the manipulation of gene activity in differentiated parafollicular C cells.

We performed parallel experiments using the $Ascl1^{CreER}$ mouse line (23) to label parafollicular C cells (Fig. 1, *T–W*). In addition to parafollicular C cells, *Ascl1* was also expressed in several neurons in the brain and scattered cells in the adrenal medulla (Fig. 1, *X–Y*) and is likely turned on at an earlier time point than CGRP during development. We found no significant differences between the efficiency and specificity of parafollicular C cell labeling between $CGRP^{CreER}$ and $Ascl1^{CreER}$. Although either mouse line would be sufficient for manipulating gene activity in parafollicular C cells, $CGRP^{CreER}$ would offer a unique opportunity to target differentiated parafollicular C cells.

Selective Inactivation of Tumor Suppressors, p53 and Rb, in Parafollicular C Cells Leads to Production of Murine Medullary Thyroid Carcinoma—To further investigate the molecular mechanisms of medullary thyroid carcinoma development, we employed the $CGRP^{CreER}$ mouse line to inactivate tumor suppressors exclusively in parafollicular C cells in adult mice. This would circumvent the issues associated with transgenic overexpression in a non-inducible fashion and persistent expression throughout embryonic development (20) or non-selective gene

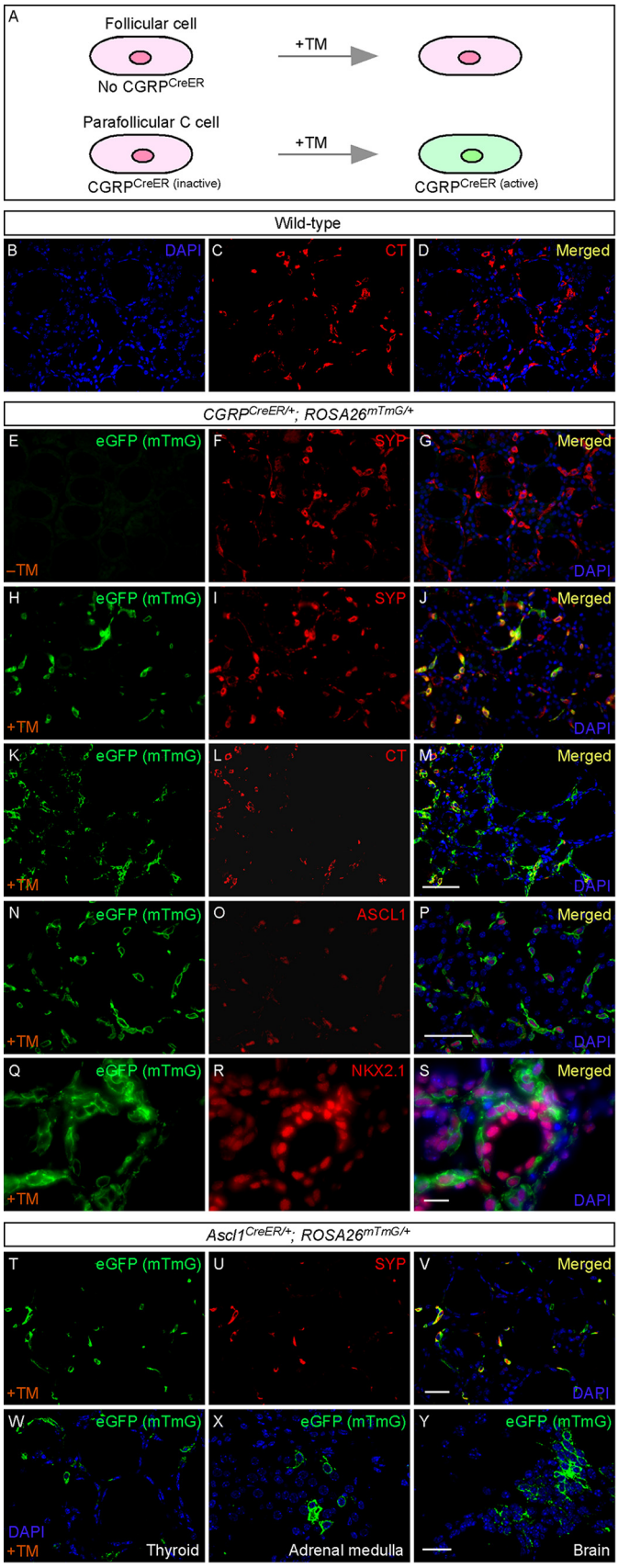

FIGURE 1. ***CGRP^{CreER}* and *Ascl1^{CreER}* mouse lines enable gene manipulation selectively in parafollicular C cells.** *A*, schematic diagram showing selective control of gene expression in parafollicular C cells using the *CGRP^{CreER}* mouse line. TM injection activates Cre and allows manipulation of gene expression. *B–D*, immunostaining of thyroid sections from wild-type adult mice. Round parafollicular C cells in the thyroid were identified by CT expression. *E–S*, immunostaining of thyroid sections from *CGRP$^{CreER/+}$; ROSA26$^{mTmG/+}$* adult mice. Extensive labeling of parafollicular C cells in the thyroid by eGFP was observed as indicated by colocalization of eGFP (*green*) and SYP (*red*), CT (*red*), or ASCL1 (*red*) signals after three TM injections. No labeled parafollicular C cells were detected in *CGRP$^{CreER/+}$; ROSA26$^{mTmG/+}$* adult mice without TM injection. NKX2.1 was detected in both columnar follicular and round parafollicular C cells. Follicular cells marked by NKX2.1 were not labeled by eGFP in *CGRP$^{CreER/+}$; ROSA26$^{mTmG/+}$* thyroid. *T–V*, immunostaining of thyroid sections from *Ascl1$^{CreER/+}$; ROSA26$^{mTmG/+}$* adult mice. Similarly, extensive labeling of parafollicular C cells in the thyroid by eGFP was observed upon TM injection. No apparent difference was discerned between *CGRP$^{CreER/+}$* and *Ascl1$^{CreER/+}$* mouse lines in this assay. *W–Y*, immunostaining of sections from the thyroid, adrenal medulla, and brain of *Ascl1$^{CreER/+}$; ROSA26$^{mTmG/+}$* adult mice. Several neurons in the brain, parafollicular C cells, and scattered cells in the adrenal medulla also displayed *Ascl1^{CreER}* activity. *Scale bars*, 50 μm for *B–M*; 50 μm for *N–P*; 10 μm for *Q–S*; 25 μm for *T–V*; and 25 μm for *W–Y*.

inactivation in the thyroid (17). We chose to ablate *p53* and *Rb*, two major tumor suppressors, in parafollicular C cells. Mice with germ line deletion of *p53* and *Rb* (in particular, *Rb*) developed multiple tumors including tumors of endocrine origin (29, 30). Our approach relies on conditional inactivation of *p53* and *Rb* by using floxed alleles of *p53* (*p53^{f}*) and *Rb* (*Rb^{f}*) (31) in which essential regions of *p53* and *Rb* would be removed to generate null alleles in the presence of Cre recombinase. We set up breeding to produce *CGRP$^{CreER/+}$; p53$^{f/f}$; Rb$^{f/f}$* mice (abbreviated as *p53$^{-/-}$*; *Rb$^{-/-}$* or double knock-out (DKO) in the figures) (Fig. 2, *A–C*). We administered tamoxifen intraperitoneally at the dose of 0.25 mg tamoxifen/g body weight daily three times to these adult animals of both sexes at 4–7 weeks of age. The mice were monitored for tumor development over a period of 12 months.

We found that selective ablation of *p53* and *Rb* in parafollicular C cells resulted in proliferation of parafollicular C cells at an early stage (for example, 1–2 months after tamoxifen injection) and tumor development shortly afterward (Fig. 2, *A*, *B*, and *D*). The phenotype is completely penetrant (100%), and a visible thyroid mass was commonly seen after 2–3 months of tamoxifen administration. These mice lost weight and exhibited labored breathing. Nearly all of them succumbed to the disease less than 6 months post-TM injection (Fig. 2*F*). For our analysis, we collected the thyroids of these mice for analysis when their general conditions required euthanasia by the approved protocol. The majority of the cohort was analyzed at ~5–6 months post-TM injection. More than 40 DKO mice were studied in this way.

Histological analysis of thyroid tumors revealed round, polygonal, or spindle cells with small, round nuclei, characteristic of medullary thyroid carcinoma (Fig. 3, *A–C* and *F–H*). Normal architecture of the thyroid was disrupted by invading tumor cells (Fig. 3, *A–C* and *F–H*), which displayed increased cell proliferation detected by either BrdU incorporation or anti-Ki67 staining (Fig. 3, *K–M*, and data not shown). The tumor cells also expressed signature markers for parafollicular C cells such as ASCL1 (MASH1) (Fig. 3, *P–R*), SYP (Fig. 3, *U–W*), and CT (data not shown). These results indicate that selective ablation of *p53* and *Rb* in parafollicular C cells results in medullary thyroid carcinoma. This not only confirms parafollicular C cells as the cells of origin for medullary thyroid carcinoma but also

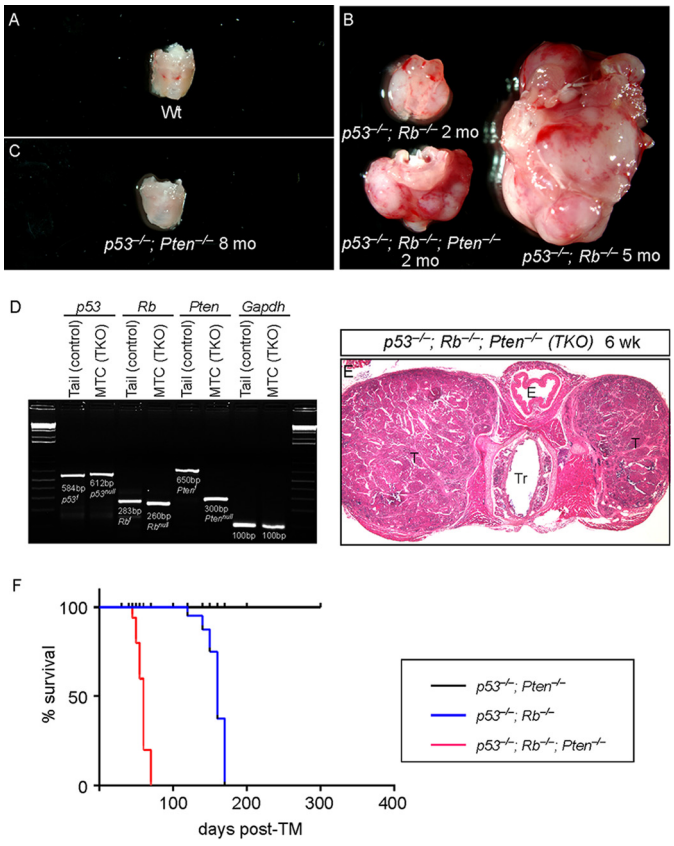

FIGURE 2. **Ablation of tumor suppressors in parafollicular C cells results in murine medullary thyroid carcinoma.** *A–C*, gross morphology of thyroid tissues dissected from representative WT, $CGRP^{CreER/+}$; $p53^{f/f}$; $Rb^{f/f}$ (abbreviated as $p53^{-/-}$; $Rb^{-/-}$), $CGRP^{CreER/+}$; $p53^{f/f}$; $Rb^{f/f}$; $Pten^{f/f}$ (abbreviated as $p53^{-/-}$; $Rb^{-/-}$; $Pten^{-/-}$), and $CGRP^{CreER/+}$; $p53^{f/f}$; $Pten^{f/f}$ (abbreviated as $p53^{-/-}$; $Pten^{-/-}$) mice at different time points post-TM injection as indicated. Thyroid tumors increased in size with time, and *p53*/*Rb*/*Pten* TKO had a higher proliferation rate than *p53*/*Rb* DKO at the same stage. Loss of *p53*/*Pten* in parafollicular C cells did not seem to exert major effects on thyroid tumor development. *D*, PCR analysis of genomic DNA derived from tails of $p53^{f/f}$; $Rb^{f/f}$; $Pten^{f/f}$ (control) animals and MTCs dissected from $p53^{-/-}$; $Rb^{-/-}$; $Pten^{-/-}$ (TKO) mice. Floxed alleles of *p53* ($p53^{f}$), *Rb* (Rb^{f}), and *Pten* ($Pten^{f}$) were converted to null alleles in thyroid tumors as indicated by the changes in PCR product size of genomic DNA. *Gapdh* serves as loading control. *E*, transverse section of medullary thyroid tumor in $p53^{-/-}$; $Rb^{-/-}$; $Pten^{-/-}$ mice. *F*, survival curves of $p53^{-/-}$; $Rb^{-/-}$, $p53^{-/-}$; $Rb^{-/-}$; $Pten^{-/-}$ and $p53^{-/-}$; $Pten^{-/-}$ mice at different time points post-TM injection as indicated. *E*, esophagus; *Tr*, trachea; *T*, thyroid tumor.

provides a new mouse model for studying the molecular basis of medullary thyroid carcinoma development.

Simultaneous Ablation of Multiple Tumor Suppressors, p53, Rb, and Pten, in Parafollicular C Cells Accelerates the Development of Murine Medullary Thyroid Carcinoma—The genetic system we developed also offers a unique opportunity to investigate the interactions between oncogenes/tumor suppressors during thyroid cancer development. In particular, the PI3K-AKT system plays a key role in RET signaling (32), and PI3K-AKT perturbation is associated with tumors of neuroendocrine tissues (33). Thus, we studied how PI3K/AKT signaling may contribute to medullary thyroid tumor development. PTEN is known to play an essential role in controlling AKT activity by opposing PI3K, and mutations in *Pten* are associated with many types of human cancers.

We investigated whether deletion of *Pten*, which mimics PI3K activation and perturbs AKT signaling, would facilitate the development of medullary thyroid carcinoma either by itself or in conjunction with loss of other tumor suppressors such as *p53* and *Rb*. Similarly, we took advantage of the conditional allele of *Pten* ($Pten^{f}$) (34) and produced $CGRP^{CreER/+}$; $p53^{f/f}$; $Rb^{f/f}$; $Pten^{f/f}$ mice (abbreviated as $p53^{-/-}$; $Rb^{-/-}$; $Pten^{-/-}$ or triple knock-out (TKO) in the figures) through mouse breeding. Tamoxifen was administered to adult $CGRP^{CreER/+}$; $p53^{f/f}$; $Rb^{f/f}$; $Pten^{f/f}$ mice to simultaneously eliminate *p53*, *Rb*, and *Pten* in parafollicular C cells. These mice developed more prominent medullary thyroid carcinoma compared with $CGRP^{CreER/+}$; $p53^{f/f}$; $Rb^{f/f}$ mice at the same stage (Fig. 2, *B*, *D*, and *E*). Similarly, the phenotype is completely penetrant (100%). These mice lost weight and exhibited labored breathing. In fact, almost all $CGRP^{CreER/+}$; $p53^{f/f}$; $Rb^{f/f}$; $Pten^{f/f}$ mice did not survive beyond 2 months post-TM administration (Fig. 2*F*). For our analysis, we collected the thyroids of these mice for analysis when their general conditions required euthanasia by the approved protocol. The majority of the cohort was analyzed at ~2 months post-TM injection. More than 50 TKO mice were investigated in this manner.

Histological analysis of *p53*/*Rb*/*Pten*-deficient tumors revealed its similarity to *p53*/*Rb* deficient tumors, including invasion of normal thyroid tissue (Fig. 3, *D* and *I*), increased cell proliferation (Fig. 3*N*), and expression of markers characteristic of parafollicular C cells including ASCL1 (MASH1) (Fig. 3*S*), SYP (Fig. 3, *Z–C′*), and CT (Fig. 3, *D′–G′*). Tumor cells also expressed NKX2.1, supporting their epithelial origin (Fig. 3, *H′–K′*). These results suggest that activation of AKT signaling by *Pten* deletion collaborates with other tumor suppressors (*e.g.* *p53* and *Rb*) and contributes to the development of medullary thyroid carcinoma.

All DKO and TKO mice perished post-TM injection in a defined time course as described above (Fig. 2*F*). These mice died most likely from a combination of thyroid dysfunction and respiratory failure, including thyroid and lung tissue destruction, obstruction of the trachea by the thyroid tumors, and adverse effects from secreted amines and peptides from neuroendocrine tumors. We did not observe any signs of metastasis of small cell lung cancer to the thyroid and vice versa at the time of our analysis.

We also examined tumor development in $CGRP^{CreER/+}$; $p53^{f/f}$; $Pten^{f/f}$ mice (abbreviated as $p53^{-/-}$; $Pten^{-/-}$ in the figures) and interestingly found no evidence of thyroid cancer development (Figs. 2*C* and 3, *E*, *J*, *O*, *T*, and *Y*) even when these mice reached 1 year of age (Fig. 2*F*). Deletion of *Pten* alone (or even with *p53*) does not appear to be sufficient in inducing medullary thyroid carcinoma. This is in contrast to the development of anaplastic thyroid tumors in *Pten*/*p53*-deficient mice (35, 36) and highlights a central role of *Rb* in medullary thyroid tumor development.

Murine Medullary Thyroid Carcinoma Is Derived from Differentiated Parafollicular C Cells—To further explore the nature of tumor-initiating cells and dissect the early events of medullary thyroid carcinoma development, we employed the $CGRP^{CreER}$ line to mark parafollicular C cells during the process of malignant transformation. This was achieved by creating mouse strains of $CGRP^{CreER/+}$; $p53^{f/f}$; $Rb^{f/f}$; $Rosa26^{mTmG/+}$ or $CGRP^{CreER/+}$; $p53^{f/f}$; $Rb^{f/f}$; $Pten^{f/f}$; $Rosa26^{mTmG/+}$ mice (abbre-

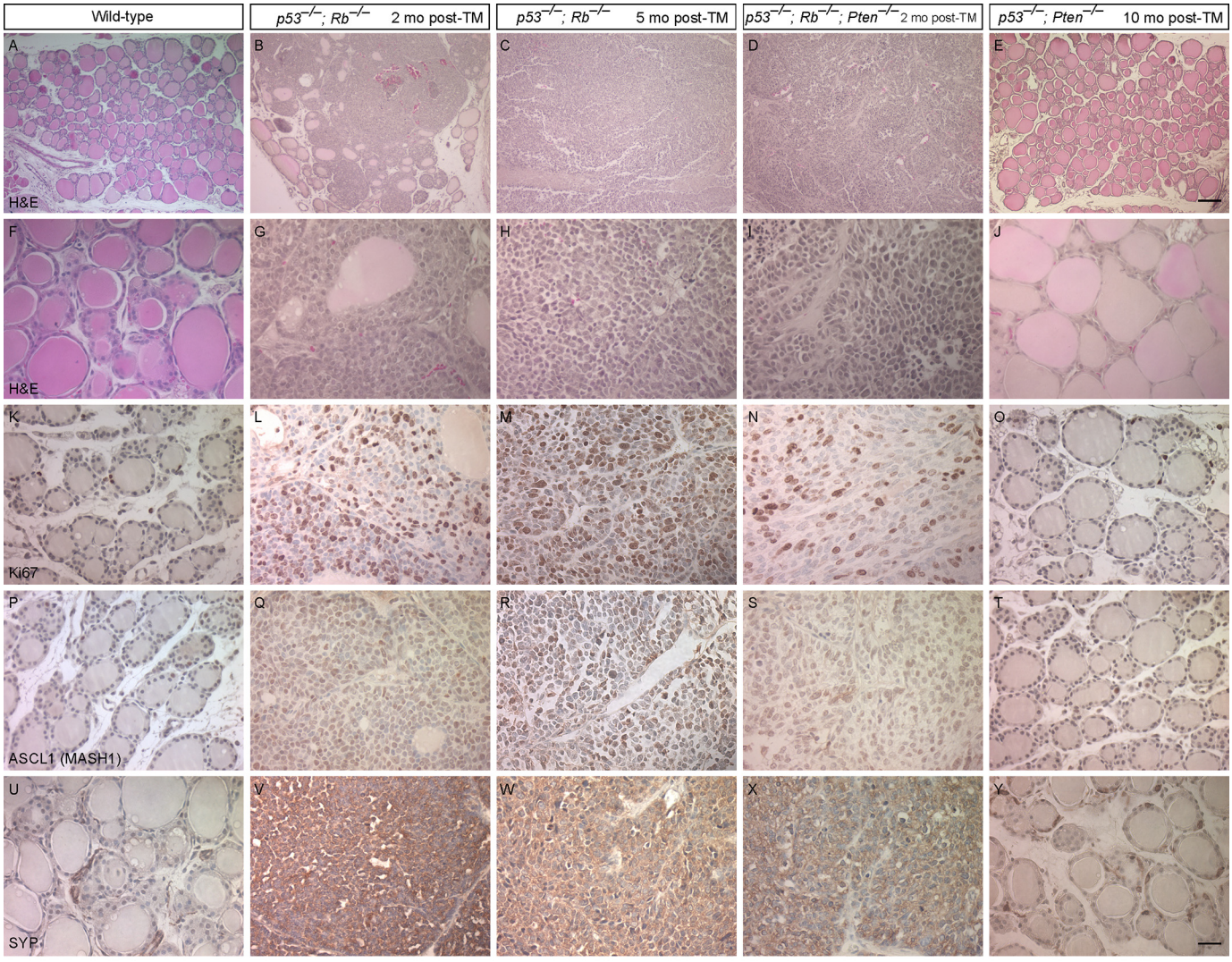
Wild-type
p53−/−; Rb−/− 2 mo post-TM
p53−/−; Rb−/− 5 mo post-TM
p53−/−; Rb−/−; Pten−/− 2 mo post-TM
p53−/−; Pten−/− 10 mo post-TM
A
B
C
D
E
H&E
F
G
H
I
J
H&E
K
L
M
N
O
Ki67
P
Q
R
S
T
ASCL1 (MASH1)
U
V
W
X
Y
SYP

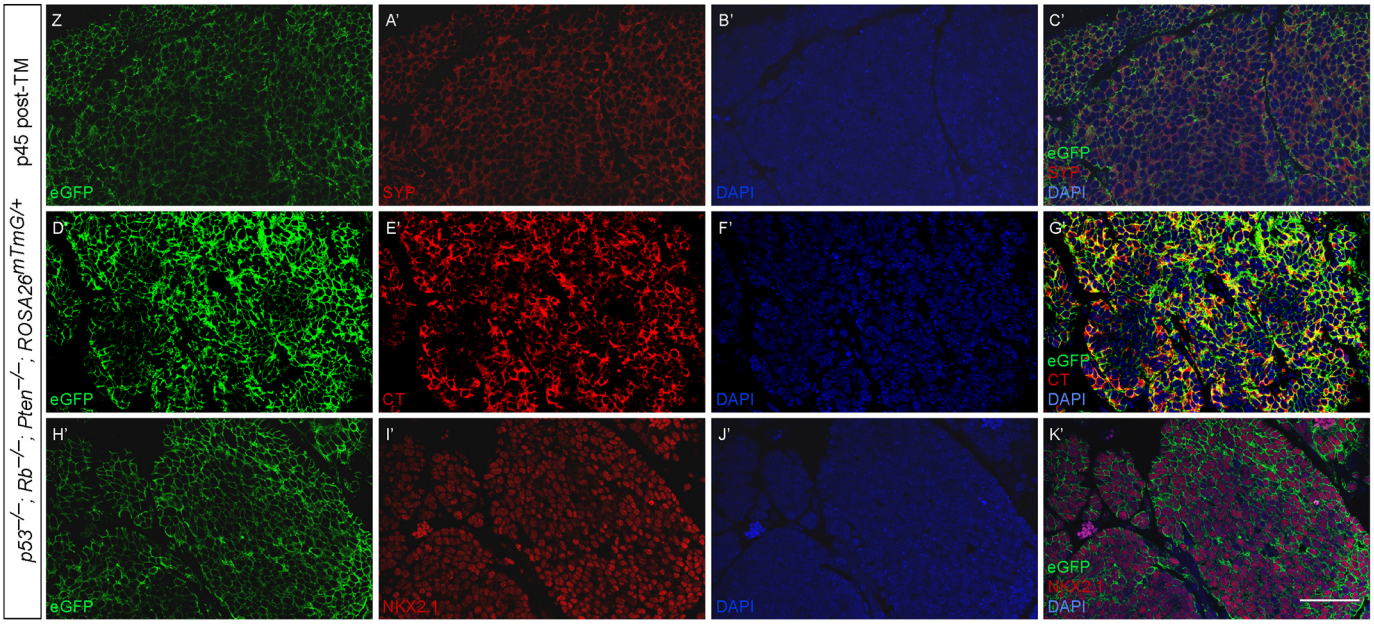
p53−/−; Rb−/−; Pten−/−; ROSA26mTmG/+ p45 post-TM
Z
A'
B'
C'
eGFP
SYP
DAPI
eGFP
SYP
DAPI
D'
E'
F'
G'
eGFP
CT
DAPI
eGFP
CT
DAPI
H'
I'
J'
K'
eGFP
NKX2.1
DAPI
eGFP
NKX2.1
DAPI

viated as $p53^{-/-}$; $Rb^{-/-}$; $ROSA26^{mTmG/+}$ and $p53^{-/-}$; $Rb^{-/-}$; $Pten^{-/-}$; $ROSA26^{mTmG/+}$, respectively, in the figure). Tamoxifen injection of $CGRP^{CreER/+}$; $p53^{f/f}$; $Rb^{f/f}$; $Rosa26^{mTmG/+}$ or $CGRP^{CreER/+}$; $p53^{f/f}$; $Rb^{f/f}$; $Pten^{f/f}$; $Rosa26^{mTmG/+}$ adult mice would label mature parafollicular C cells with eGFP (from the $Rosa26^{mTmG}$ allele) in addition to inactivating *p53*/*Rb* or *p53*/*Rb*/*Pten*. Medullary thyroid carcinoma developed in $CGRP^{CreER/+}$; $p53^{f/f}$; $Rb^{f/f}$; $Rosa26^{mTmG/+}$ or $CGRP^{CreER/+}$; $p53^{f/f}$; $Rb^{f/f}$; $Pten^{f/f}$; $Rosa26^{mTmG/+}$ mice in a manner identical to that in $CGRP^{CreER/+}$; $p53^{f/f}$; $Rb^{f/f}$ and $CGRP^{CreER/+}$; $p53^{f/f}$; $Rb^{f/f}$; $Pten^{f/f}$ mice.

Analysis of thyroid tumors in $CGRP^{CreER/+}$; $p53^{f/f}$; $Rb^{f/f}$; $Rosa26^{mTmG/+}$ or $CGRP^{CreER/+}$; $p53^{f/f}$; $Rb^{f/f}$; $Pten^{f/f}$; $Rosa26^{mTmG/+}$ mice revealed that almost all tumor cells were labeled by eGFP a few months after TM injection (Fig. 4, *A–C*, and data not shown). To determine the origin of these labeled tumor cells, we traced tumor development to earlier stages. Extensive labeling of parafollicular C cells by eGFP was apparent even at 1 week post-TM injection in $CGRP^{CreER/+}$; $p53^{f/f}$; $Rb^{f/f}$; $Rosa26^{mTmG/+}$ or $CGRP^{CreER/+}$; $p53^{f/f}$; $Rb^{f/f}$; $Pten^{f/f}$; $Rosa26^{mTmG/+}$ mice (Fig. 4, *D–I*). Importantly, many of these eGFP-labeled parafollicular C cells in $CGRP^{CreER/+}$; $p53^{f/f}$; $Rb^{f/f}$; $Rosa26^{mTmG/+}$ or $CGRP^{CreER/+}$; $p53^{f/f}$; $Rb^{f/f}$; $Pten^{f/f}$; $Rosa26^{mTmG/+}$ mice were proliferating in comparison with the quiescence of eGFP-labeled cells in $CGRP^{CreER/+}$; $Rosa26^{mTmG/+}$ mice (Fig. 4, *J–L*). Proliferation of parafollicular C cells led to medullary thyroid tumors in which all tumor cells were labeled by eGFP (Fig. 4, *A–C*, and data not shown). The proliferation rate of eGFP-labeled parafollicular C cells was higher in *p53*/*Rb*/*Pten* triple knock-out mice than *p53*/*Rb* double knock-out mice during the process of parafollicular C cell hyperplasia (Fig. 4*M*). These results suggest that mature parafollicular C cells underwent hyperplasia caused by the loss of tumor suppressors and subsequently led to tumor formation. Our system provides a unique opportunity to study the initial events of medullary thyroid tumor development.

Human and Murine Medullary Thyroid Carcinoma Displays Active PI3K/AKT Signaling—Recent studies have shown that the PI3K/AKT pathway is involved in neuroendocrine tumor initiation and progression including medullary thyroid carcinoma (33). We first examined phospho-AKT (Ser^{473}) (pAKT) status in 10 primary human medullary thyroid carcinoma samples. pAKT was robustly expressed in 80% (8 of 10) of medullary thyroid carcinoma samples (Fig. 5*C*) but not in normal human thyroid tissues (Fig. 5*A*). All of the tumors displayed neuroendocrine features and stained positive for neuroendocrine markers such as SYP (Fig. 5*B*). These findings suggest that the PI3K/AKT pathway is active in the majority human medullary thyroid carcinoma.

The PI3K/AKT signaling pathway is expected to be active after *Pten* elimination. Therefore, we assessed PI3K/AKT signaling by examining pAKT expression using immunohistochemistry in our mouse models. Strong pAKT signals were present in TKO tumors at 2 months post-TM administration (Fig. 5, *E* and *F*). Weaker pAKT signals were also observed in DKO tumors at 5 months post-TM administration (Fig. 5*D*). These data support a model in which loss of *Pten* activates PI3K/AKT signaling and facilitates tumor progression of *p53*/*Rb*-deficient medullary thyroid tumors.

RNA-Seq Analysis of Murine Medullary Thyroid Carcinoma Reveals Genes and Pathways Perturbed Because of Loss of Tumor Suppressors—As a first step toward uncovering the molecular mechanisms that underlie the pathogenesis of medullary thyroid carcinoma, we performed RNA-Seq analysis on medullary thyroid tumors derived from $CGRP^{CreER/+}$; $p53^{f/f}$; $Rb^{f/f}$; $Pten^{f/f}$ mice. RNA from wild-type thyroid instead of parafollicular C cells was used as a control because it is challenging to isolate an adequate number of wild-type parafollicular C cells. We validated differential gene expression caused by loss of tumor suppressors by qPCR analysis.

Ingenuity Pathway Analysis (IPA) of RNA-Seq data identified a number of canonical pathways that were enriched in the differentially expressed genes (Fig. 6*A*). Among the top pathways enriched are cAMP-mediated signaling, actin cytoskeleton signaling, G protein-coupled receptor (GPCR) signaling, liver X receptor (LXR)/retinoid X receptor (RXR) activation, and integrin-linked kinase signaling. Moreover, thyroid cancer signaling and thyroid hormone receptor/RXR activation were also enriched. Interestingly, the LXR/RXR pathway was activated, whereas cAMP-mediated signaling, actin cytoskeleton signaling, and integrin-linked kinase signaling were inhibited in medullary thyroid tumors (Fig. 6*A*). These findings form the basis of future mechanistic studies to understand how these pathways may confer tumor properties.

We also asked whether major signaling pathways were perturbed in medullary thyroid tumors. Although most major signaling pathways were down-regulated, we found that the expression levels of *Axin2*, indicative of Wnt pathway activation, was elevated (Fig. 6*B*). Similarly, this insight will enable studies to uncover the molecular basis of how major signaling pathways control tumor development and survival. Analysis of genes whose expression was altered in medullary thyroid tumors (Fig. 7*A*) could provide tumor biomarkers and important drivers of tumorigenesis.

FIGURE 3. **Histological and marker analysis of murine medullary thyroid carcinoma.** *A–J*, hematoxylin-eosin (*H&E*) staining of thyroid sections derived from wild-type, $CGRP^{CreER}/+$; $p53^{f/f}$; $Rb^{f/f}$ (abbreviated as $p53^{-/-}$; $Rb^{-/-}$), $CGRP^{CreER}/+$; $p53^{f/f}$; $Rb^{f/f}$; $Pten^{f/f}$ (abbreviated as $p53^{-/-}$; $Rb^{-/-}$; $Pten^{-/-}$), and $CGRP^{CreER}/+$; $p53^{f/f}$; $Pten^{f/f}$ mice (abbreviated as $p53^{-/-}$; $Pten^{-/-}$) at time points post-TM as indicated. Parafollicular C cell hyperplasia was evident in *p53*/*Rb* DKO thyroids at 2 months post-TM, and remnants of thyroid follicles could still be found at the periphery of the thyroid. By 5 months post-TM in *p53*/*Rb* DKO thyroids and by 2 months post-TM in *p53*/*Rb*/*Pten* TKO thyroids, the entire thyroid gland had been replaced by tumor cells, and almost no normal thyroid tissue could be found. By contrast, the histology of *p53*/*Pten* DKO thyroid is similar to that in wild type. *K–Y*, immunostaining of thyroid sections derived from wild-type, *p53*/*Rb* DKO, *p53*/*Rb*/*Pten* TKO, and *p53*/*Pten* DKO mice at time points post-TM as indicated. Tumor cells in *p53*/*Rb* DKO and *p53*/*Rb*/*Pten* TKO thyroids expressed markers of parafollicular C cells such as SYP and ASCL1 (MASH1) and were highly proliferative as judged by Ki67 staining. *Z–K′*, immunofluorescence of thyroid sections derived from $p53^{-/-}$; $Rb^{-/-}$; $Pten^{-/-}$; $ROSA26^{mTmG/+}$ mice at the time point post-TM as indicated. Tumor cells expressed markers of parafollicular C cells such as SYP and CT. Tumor cells also expressed NKX2.1, indicating the origin of tumors from thyroid tissues. *Scale bars*, 12.5 μm for *A–E*; 50 μm for *F–Y*; and 50 μm for *Z–K′*.

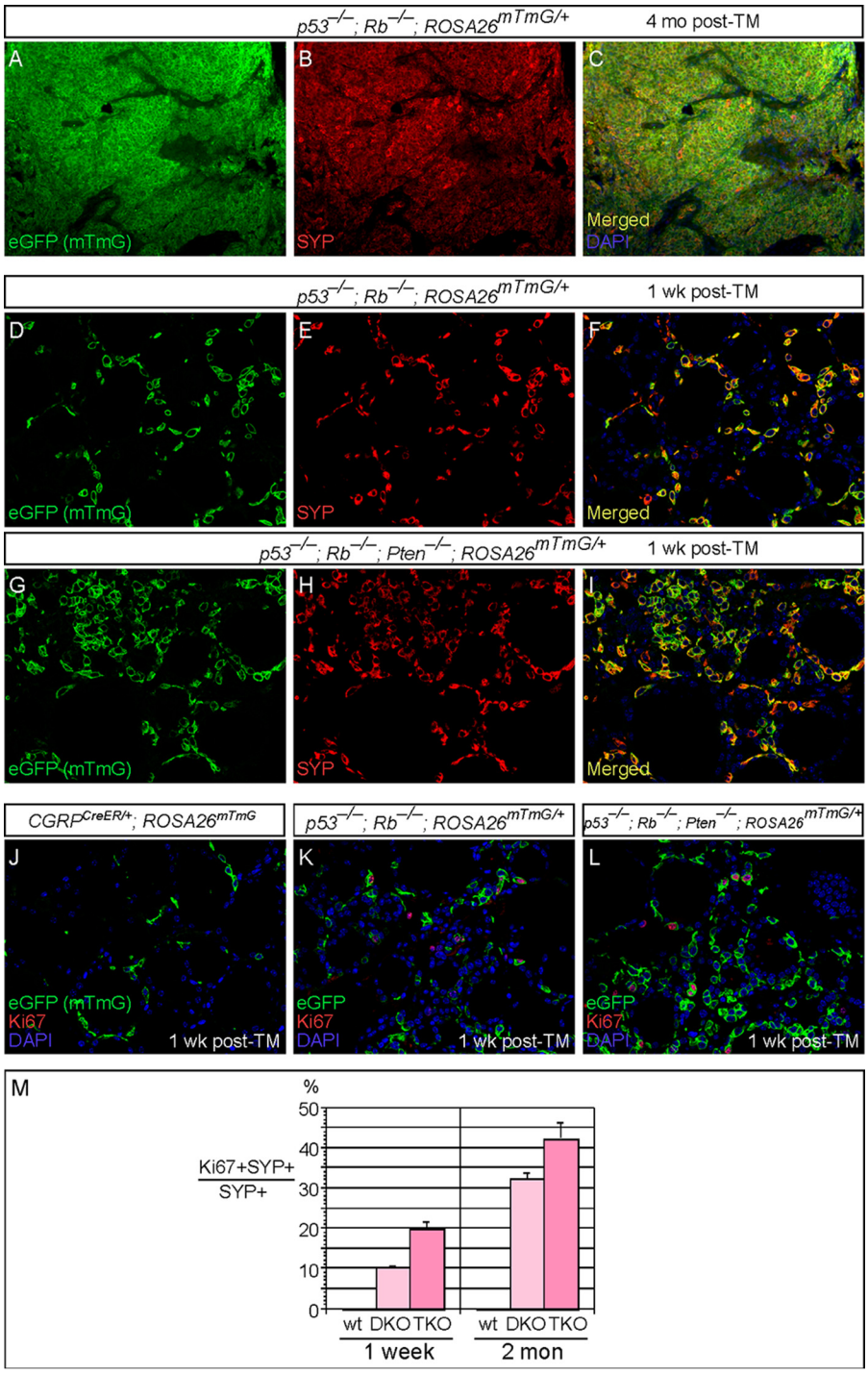

FIGURE 4. **Tracing of labeled parafollicular C cells during medullary thyroid tumor development.** *A–L*, immunostaining of thyroid sections from *CGRP*$^{CreER/+}$; *p53*$^{f/f}$; *Rb*$^{f/f}$; *ROSA26*$^{mTmG/+}$ (abbreviated as *p53*$^{-/-}$; *Rb*$^{-/-}$; *ROSA26*$^{mTmG/+}$) and *CGRP*$^{CreER/+}$; *p53*$^{f/f}$; *Rb*$^{f/f}$; *Pten*$^{f/f}$; *ROSA26*$^{mTmG/+}$ (abbreviated as *p53*$^{-/-}$; *Rb*$^{-/-}$; *Pten*$^{-/-}$; *ROSA26*$^{mTmG/+}$) mice. Tamoxifen injection selectively ablated *p53*/*Rb* (*A–F*) or *p53*/*Rb*/*Pten* (*G–I*) in parafollicular C cells, which were simultaneously labeled by eGFP (from *ROSA26*^{mTmG}). Proliferating parafollicular C cells could be found even at 1 week after TM injection in the thyroid glands of both *CGRP*$^{CreER/+}$; *p53*$^{f/f}$; *Rb*$^{f/f}$; *ROSA26*$^{mTmG/+}$ (*K*) and *CGRP*$^{CreER/+}$; *p53*$^{f/f}$; *Rb*$^{f/f}$; *Pten*$^{f/f}$; *ROSA26*$^{mTmG/+}$ (*L*) mice. At 4 months post-TM in *p53*/*Rb* DKO thyroids, most, if not all, tumor cells were eGFP^{+}, suggesting that these tumor cells were derived from eGFP-labeled parafollicular C cells. *M*, quantification of proliferating parafollicular C cells in *p53*/*Rb* DKO and *p53*/*Rb*/*Pten* TKO thyroids. Three mice were counted for each genotype at a given time point. A total 152 DKO and 178 TKO SYP^{+} cells were counted at 1 week post-TM, and a total of 1386 DKO and 1427 TKO SYP^{+} cells were counted at 2 months post-TM. The ratio of Ki67^{+}; SYP^{+} and SYP^{+} cells is represented as means ± S.E. *p* value = 0.0017 (comparison between DKO and TKO at 1 week post-TM) and *p* value = 0.016 (comparison between DKO and TKO at 2 months post-TM).

Ingenuity Core analysis identified several gene networks with significant alterations in medullary thyroid tumors. The highest scoring network centered almost completely on GPCR as a hub (Fig. 7*B*), highlighting its potential role in thyroid tumor development. To examine the cause of transcriptional alterations in thyroid tumors, we performed regulator effects analysis using IPA. The regulator effects analysis not only identifies upstream regulators of genes with altered expression in RNA-Seq but also

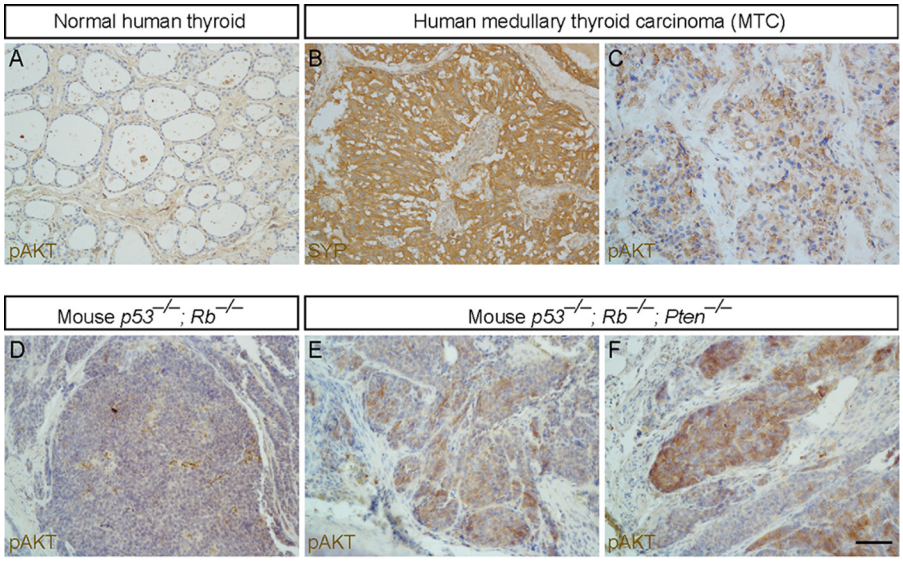

FIGURE 5. **Active PI3K/AKT signaling in murine and human medullary thyroid carcinoma.** *A–C*, immunostaining of human thyroid sections. Compared to normal human thyroid tissues (*A*), human medullary thyroid carcinoma had robust expression of neuroendocrine markers such as SYP (*B*). Among the 10 samples of human medullary thyroid carcinoma examined, eight of them had strong staining of phospho-AKT (Ser^{473}) (pAKT) (*C*), whereas two had weaker pAKT staining. This is consistent with active PI3K/AKT signaling in human medullary thyroid carcinoma. *D–F*, similarly, thyroid tumors derived from *p53*/*Rb* DKO mice at 5 months post-TM also showed weak pAKT staining (*D*). By contrast, strong pAKT signals were detected in *p53*/*Rb*/*Pten* TKO thyroids even at 2 months post-TM (*E* and *F*). *Scale bars*, 50 μm for *A–F*.

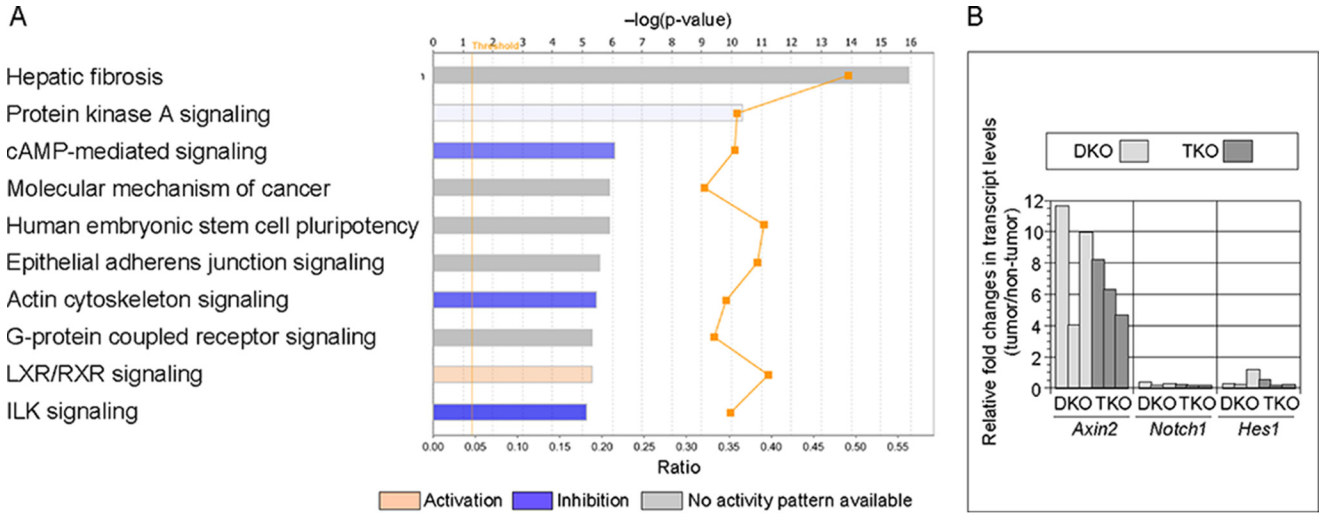

FIGURE 6. **RNA-Seq analysis of medullary thyroid carcinoma induced by removal of tumor suppressors.** *A*, top canonical pathways that were enriched in differentially expressed genes. Among the top pathways are cAMP-mediated signaling (*p* value = 8.32E-07, *z* score = 2.9), actin cytoskeleton signaling (*p* value = 3.31E-06, *z* score = −3.3), LXR/RXR activation (*p* value = 4.68E-06, *z* score = 0.949), and G protein-coupled receptor signaling (*p* value = 4.57E-06). Importantly, thyroid cancer signaling and thyroid hormone receptor/RXR activation are also enriched (*p* value = 6.61E-05, and *p* value = 7.94E-05, respectively) (not shown). *B*, qPCR analysis of RNA extracted from thyroid tumors derived from $CGRP^{CreER/+}$; $p53^{f/f}$; $Rb^{f/f}$ (DKO) or $CGRP^{CreER/+}$; $p53^{f/f}$; $Rb^{f/f}$; $Pten^{f/f}$ (TKO) adult mice injected with tamoxifen. Wild-type thyroid tissue was used as a control. Target genes for each major signaling pathway were assessed for changes in their expression in tumor *versus* non-tumor tissues. The numbers represent fold of changes in tumor tissues. Tumors from multiple mice were analyzed. The expression levels of *Axin2*, *Hes1*, and *Notch1* genes in thyroid tumors were graphed as fold of changes relative to wild-type thyroid tissues.

connects these genes with known homeostatic and disease processes. The top regulator identified by IPA is Ccl11. Reduced *Ccl11* expression as revealed by RNA-Seq could lower the expression of *Bmp6*, *Cxcl12*, *Dpp4*, *Fas*, *Fgf10*, *Icam*1, *Itga1*, *Itgam*, *Itgb1*, *Lep*, and *Vegfc*, consequently inhibiting multiple processes including adhesion of tumor cells, vascularization, and activation of leukocytes (Fig. 7*C*). Genome-wide expression analysis of medullary thyroid tumor thus is a productive way to reveal the molecular underpinnings of various aspects of tumor biology.

Discussion

Medullary thyroid carcinomas are prone to early metastasis, severely limiting treatment options for patients with extensive disease. This underscores the urgent issue of identifying new drug targets for treating medullary thyroid carcinomas. Because *RET* mutations (denoted RET(+)) have been well documented in hereditary medullary thyroid carcinoma and in a significant fraction of sporadic medullary thyroid carcinoma, inhibitors of RET are proven for clinical use in treating these patients (37, 38). Conceivably, tumor cells would eventually

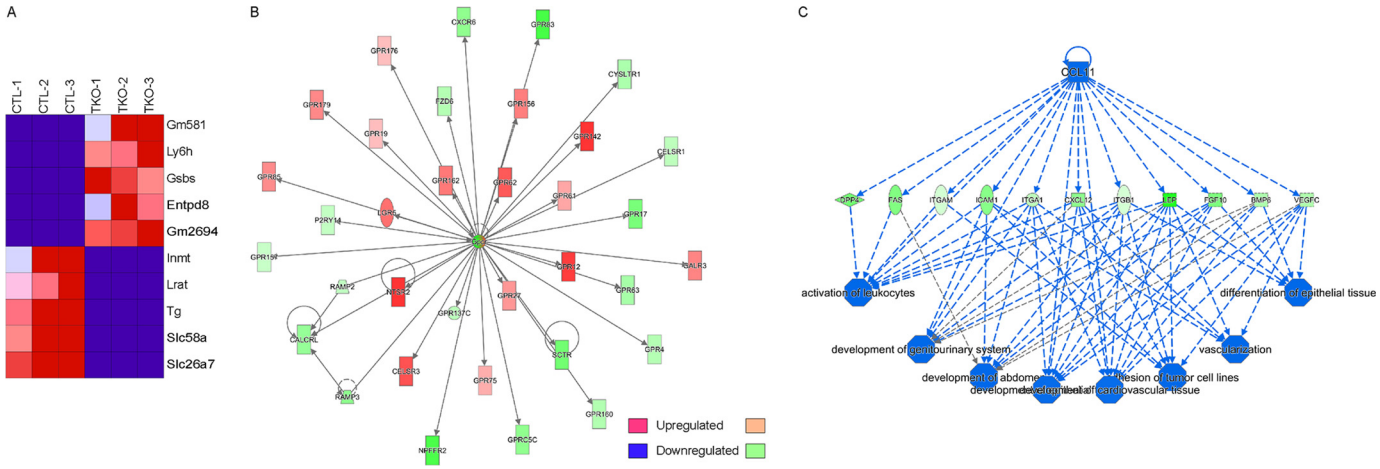

FIGURE 7. **Heat map analysis, gene network analysis, and regulator effects analysis of medullary thyroid carcinoma.** *A*, heat map analysis of the highly up-regulated (*red*) and down-regulated (*blue*) genes in thyroid tumors (TKO) compared with controls (*CTL*). Only genes at the top of the list were shown. *B*, gene network analysis of genes identify in RNA-Seq of thyroid tumors. GPCR signaling is the top network identified by IPA (score = 30). *C*, regulator effects analysis by IPA identified a top upstream regulator in Ccl11. Inhibition of *Ccl11* could lower expression of *Bmp6*, *Cxcl12*, *Dpp4*, *Fas*, *Fgf10*, *Icam1*, *Itga1*, *Itgam*, *Itgb1*, *Lep*, and *Vegfc* and consequently disrupt multiple processes including adhesion of tumor cells, vascularization, and activation of leukocytes.

develop resistance to RET inhibitors as has been observed in other types of cancers that are initially sensitive to receptor tyrosine kinase inhibitors (39). This could be due to second site mutations in receptor tyrosine kinases, a shift toward dependence on other genes or signaling pathways for tumor survival, or even epithelial to mesenchymal transition, all of which could confer resistance. These obstacles highlight a central issue of identifying new genes and pathways that are perturbed during tumor development or progression.

In this study, we created mouse models of medullary thyroid carcinoma in which tumor development followed a defined time sequence upon removal of tumor suppressors. Our findings suggest that major tumor suppressors, such as *p53*, *Rb*, and *Pten*, could interact and play a key role in the development of RET(−) medullary thyroid tumors. Furthermore, even in RET(+) medullary thyroid tumors, tumor suppressors may contribute to tumor phenotypes including tumor progression and metastasis.

Our RNA-Seq analysis of murine medullary thyroid carcinoma uncovered a significant number of genes, the expression of which was perturbed because of a loss of major tumor suppressors. Moreover, several pathways were also perturbed in murine thyroid tumor tissues. In fact, microarray analysis of human medullary thyroid carcinoma has uncovered a number of these pathways (40). This further validates our mouse model for understanding the molecular basis of medullary thyroid tumor development and metastasis. A major challenge in genome-wide mutational or transcript analysis is to reveal the *in vivo* function of gene mutations or gene/pathway activation and repression. CRISPR technology could provide an efficient method to investigate how one or more of these genes and pathways mediate the effects of tumor suppressors during medullary thyroid tumor development. It is interesting to note that CDK5 has been identified as an upstream regulator of RB in medullary thyroid carcinoma (41). This provides an opportunity to investigate whether CDK5 controls genes and pathways unveiled in our expression analysis.

We used RNA from wild-type thyroid as controls for RNA-Seq of medullary thyroid carcinoma. It is technically difficult to isolate a sufficient number of wild-type parafollicular C cells as controls. Use of wild-type thyroids as controls could have affected the analysis of RNA-Seq data of thyroid cancer. For instance, genes that are up-regulated in medullary thyroid tumors may have been missed in our analysis if they are also expressed in cells in the thyroid other than parafollicular C cells. In addition, genes with low levels of expression in parafollicular C cells will be underrepresented in wild-type thyroid, and this could lead to false identification of up-regulated genes in medullary thyroid carcinoma. Nevertheless, we speculate that many tumor-related transcripts would still have been uncovered in our approach.

Interestingly, we found that Wnt and Notch signaling is perturbed in response to loss of tumor suppressors. Activation of Wnt signaling has been associated with anaplastic thyroid cancer and in some cases papillary or follicular thyroid tumors (42). Increased Wnt target gene expression in our mouse model of medullary thyroid carcinoma suggests that Wnt pathway activation could be a general mechanism that contributes to thyroid tumor development. Consistent with this, up-regulation of DKK4 (Dickkopf-related protein 4) associated with Wnt pathway activation was reported in human medullary thyroid carcinoma carrying the RET^{M918T} mutation (40).

Our finding of reduced Notch signaling in medullary thyroid carcinoma is consistent with a previous report in which Notch signaling is silent in medullary or anaplastic thyroid tumors and activation of Notch signaling reduces tumor growth (43, 44). This is also in agreement with the observation that down-regulation of Notch signaling is associated with neuroendocrine cell differentiation during development. Further analysis of how these signaling pathways control tumor cell properties will offer new insight into changes in signaling networks during tumor evolution (45).

Our mouse model also provides a unique opportunity to identify genes disrupted at different stages of medullary thyroid

tumor development, a task not feasible if human tumor tissues are used. This is particularly relevant for investigating early tumor development. Because parafollicular C cells are labeled by eGFP upon tamoxifen administration in our genetic system, proliferating C cells can be isolated by FACS for expression and genomic analysis including RNA-Seq and Exome sequencing. Such analysis can identify markers for early diagnosis of medullary thyroid carcinoma. Moreover, driver mutations required for tumor growth, survival, progression, and metastasis can be uncovered, offering potential candidates for designing new targeted therapies or developing other types of therapies. Complementary to these efforts, we will derive cell lines from medullary thyroid carcinomas, which will provide a platform for screening small molecules that control tumor growth or apoptosis.

Development of medullary thyroid carcinoma in our mouse model, in which tumor suppressors are inactivated selectively in differentiated parafollicular C cells in adult mice, provides insight into the early stages of medullary thyroid carcinoma development. Our work complements previous studies in which transgenic overexpression of mutant RET protein under the control of a 2-kb *CT*/*CGRP* promoter led to development of medullary thyroid carcinoma in mice (20). In this system, mutant RET protein is overexpressed in all cells that activate the 2-kb *CT*/*CGRP* promoter during thyroid development and in adult life. Our findings are consistent with a model in which medullary thyroid tumors can initiate in mature parafollicular C cells that proliferate in response to loss of tumor suppressors or other genetic perturbations. Nevertheless, we cannot completely exclude the possibilities that medullary thyroid carcinoma can also be derived from a small number of unidentified progenitors or stem cells or be transdifferentiated from other cell types. Without markers available to label and follow the fate of early progenitors that give rise to parafollicular C cells, this issue cannot be unambiguously resolved.

Experimental Procedures

Materials—Mouse lines. All animal work was carried out in strict accordance with the recommendations in the Guide for the Care and Use of Laboratory Animals of the National Institutes of Health. The protocol was approved by the Institutional Animal Care and Use Committee at the University of California, San Francisco.

CGRP^{CreER} mice were generated by gene targeting to introduce CreER into the endogenous *Calca* locus as described (22). *p53* floxed (*p53*^{f}) (FVB.129-*Trp53*^{tm1Brn}) and *Rb* floxed (*Rb*^{f}) (FVB;129-*Rb1*^{tm2Brn}) mice were obtained from the NCI Mouse Repository. *Pten* floxed (*Pten*^{f}) (C;129S4-*Pten*^{tm1Hwu}/J), *ROSA26*^{mTmG} (Stock *Gt(ROSA)26Sor*$^{tm4(ACTB-tdTomato,-EGFP)Luo}$/J), *R26R* (B6; 129S4-*Gt(ROSA)26Sor*^{tm1Sor}/J), and *Ascl1*^{CreER} (STOCK *Ascl1*$^{tm1.1(Cre/ERT2)Jejo}$/J) mice were obtained from the Jackson Laboratory. The following primers for mouse genes were used for PCR genotyping of the conversion of a conditional (floxed) allele to a null allele: *Gapdh* (forward, 5′-AGGTTGTCTCCTGCGACTTCA-3′; reverse, 5′-CCAGGAAATGAGCTTGACAAAGTT-3′), *p53* (forward, 5′-CACAAAAACAGGTTAAACCCA-3′; forward, 5′-AAGGGGTATGAGGGACAAGG-3′; reverse, 5′-GAAGACAGAAAAGGGGAGGG-3′), *Rb* (forward, 5′-GGCGTGTGCCATCAATG-3′; reverse, 5′-GAAAGGAAAGTCAGGGACATTGGG-3′; reverse, 5′-CTCAAGAGCTCAGACTCATGG-3′), and *Pten* (forward, 5′-TCCCAGAGTTCATACCAGGATTTAAG-3′; reverse, 5′-AATCTGTGCATGAAGGGAACACGTCA-3′; reverse, 5′-GCAATGGCCAGTACTAGTGAAC-3′).

Tamoxifen (Sigma) stock solution was dissolved in Mazola corn oil (Sigma) at 50 mg/ml. Adult mice (4–7 weeks old) of both sexes were injected intraperitoneally with 0.25 mg tamoxifen/g body weight daily three times. The mice were monitored for tumor development over a period of 12 months.

Immunohistochemistry—Mouse thyroids and thyroid tumors were dissected and fixed overnight at 4 °C in 2% paraformaldehyde. Tissues were embedded in paraffin wax and sectioned at 6 μm or embedded in OCT and sectioned at 10 μm. Human medullary thyroid carcinoma samples were purchased from Fanpu Biotech, Inc. (Guilin, China). Histological analysis was performed as described (22).

Histology and immunohistochemistry was performed following standard procedures. The following primary antibodies were used: chicken anti-GFP (1:200; Abcam catalog no. ab13970), rabbit anti-CGRP (1:400; Sigma catalog no. C8198), Ki67 (1:200; BD Biosciences catalog no. 550609), rabbit anti-SYP (prediluted; Life Technologies catalog no. 08-0130), rabbit anti-CT (1:100; Agilent catalog no. A057601–2), rabbit anti-NKX2.1 (1:200; Epitomics catalog no. 2044–1), mouse anti-ASCL1 (MASH1) (1:200; BD Biosciences catalog no. 556604), and phospho-AKT (Ser^{473}) (D9E) rabbit mAb (1:100; Cell Signaling Technologies catalog no. 4060). Secondary antibodies and conjugates used included donkey anti-chick DyLight 488 (1:1000; Jackson ImmunoResearch Laboratories), donkey anti-rabbit Alexa Fluor 594 (1:1000; Life Technologies), donkey anti-mouse AlexaFluor 594 (1:1000; Life Technologies), and DAPI (1:10,000; Sigma). For the visualization of biotinylated secondary antibodies (goat anti-rabbit, 1:1000 and goat anti-mouse, 1:1,000; Jackson ImmunoResearch Laboratories), we used streptavidin-horseradish peroxidase (Jackson ImmunoResearch Laboratories) and diaminobenzidine as a chromogen.

Fluorescent images were acquired using a SPOT 2.3 camera connected to a Nikon E1000 epifluorescence microscope. Adjustment of RGB histograms and channel merges were performed using Advanced SPOT. Confocal images were captured on a Leica laser-scanning confocal microscope. Adjustment of red/green/blue histograms and channel merges were performed using ImageJ.

qPCR—Wild-type thyroid and medullary thyroid tumor tissues from *CGRP*$^{CreER/+}$; *p53*$^{f/f}$; *Rb*$^{f/f}$ or *CGRP*$^{CreER/+}$; *p53*$^{f/f}$; *Rb*$^{f/f}$; *Pten*$^{f/f}$ mice were dissected and homogenized using a glass homogenizer in TRIzol reagent (Life Technologies). RNA was purified through an RNeasy mini-spin column (Qiagen). RNA was eluted in water and examined with NanoDrop spectrophotometer and Agilent Bioanalyzer. 1 μg of total RNA from each sample was reverse transcribed using SuperScript III First-Strand Synthesis System (Life Technologies). qPCR was performed with SYBR Green system (Roche) in an ABI Prism 7900HT sequence detection system.

The following primers for mouse genes were used: *Gapdh* (forward, 5′-CATCACTGCCACCCAGAAGACTG-3′; reverse,

5′-ATGCCAGTGAGCTTCCCGTTCAG-3′), *Axin2* (forward, 5′-ATGGAGTCCCTCCTTACCGCAT-3′; reverse, 5′-GTTCCACAGGCGTCATCTCCTT-3′), *Notch1* (forward, 5′-GCTGCCTCTTTGATGGCTTCGA-3′; reverse, 5′-CACATTCGGCACTGTTACAGCC-3′), and *Hes1* (forward, 5′-GGAAATGACTGTGAAGCACCTCC-3′; reverse, 5′-GAAGCGGGTCACCTCGTTCATG-3′).

RNA-Seq of Thyroid Tumors—Thyroid tumors were dissected from $CGRP^{CreER/+}$; $p53^{f/f}$; $Rb^{f/f}$ or $CGRP^{CreER/+}$; $p53^{f/f}$; $Rb^{f/f}$; $Pten^{f/f}$ mice, and RNA was extracted using a combination of TRIzol (Life Technologies) and RNeasy kit (Qiagen). RNA quality was evaluated using the Agilent 2100 bioanalyzer (Agilent Technologies). Only intact RNA (RNA integrity number over 9) was used for RNA-Seq analysis. RNA from wild-type thyroid was used as controls. It is not feasible to isolate a sufficient number of wild-type parafollicular C cells as controls.

Paired end libraries were prepared using the SureSelect strand-specific RNA library prep kit (Agilent Technologies). Multiplexed sequencing was run in a HiSeq2000 sequencer (Illumina). Read alignment and gene expression levels were analyzed by the Maverix analytic platform (Maverix).

The pathway enrichment analysis, the network analysis, and the upstream regulator analysis were performed on differentially expressed genes using Ingenuity Pathway Analysis (Ingenuity Systems, Redwood City, CA). The data set was culled from differentially expressed genes with a cutoff of at least a 2-fold change in expression levels (p value ≤ 0.001). The heat map image was generated using the HeatMapImage module of the GenePattern program from the Broad Institute.

Author Contributions—H. S. performed all the experiments with assistance from C. L., E. Y., K. Z., and X. L. H. S., E. Y., and P.-T. C. wrote the manuscript.

Acknowledgments—We thank members of the Chuang laboratory for helpful discussions.

References

1. Cabanillas, M. E., McFadden, D. G., and Durante, C. (2016) Thyroid cancer. *Lancet* **388,** 2783–2795
2. Matias-Guiu, X., and De Lellis, R. (2014) Medullary thyroid carcinoma: a 25-year perspective. *Endocr. Pathol.* **25,** 21–29
3. Almeida, M. Q., and Hoff, A. O. (2012) Recent advances in the molecular pathogenesis and targeted therapies of medullary thyroid carcinoma. *Curr. Opin. Oncol.* **24,** 229–234
4. Wells, S. A., Jr, Asa, S. L., Dralle, H., Elisei, R., Evans, D. B., Gagel, R. F., Lee, N., Machens, A., Moley, J. F., Pacini, F., Raue, F., Frank-Raue, K., Robinson, B., Rosenthal, M. S., Santoro, M., *et al.* (2015) Revised American Thyroid Association guidelines for the management of medullary thyroid carcinoma. *Thyroid* **25,** 567–610
5. Maxwell, J. E., Sherman, S. K., O'Dorisio, T. M., and Howe, J. R. (2014) Medical management of metastatic medullary thyroid cancer. *Cancer* **120,** 3287–3301
6. Ernani, V., Kumar, M., Chen, A. Y., and Owonikoko, T. K. (2016) Systemic treatment and management approaches for medullary thyroid cancer. *Cancer Treat. Rev.* **50,** 89–98
7. Nikiforov, Y. E. (2016) Thyroid cancer in 2015: molecular landscape of thyroid cancer continues to be deciphered. *Nat. Rev. Endocrinol.* **12,** 67–68
8. Xing, M. (2013) Molecular pathogenesis and mechanisms of thyroid cancer. *Nat. Rev. Cancer* **13,** 184–199
9. Bikas, A., Vachhani, S., Jensen, K., Vasko, V., and Burman, K. D. (2016) Targeted therapies in thyroid cancer: an extensive review of the literature. *Exp. Rev. Clin. Pharmacol.* **9,** 1299–1313
10. Pozo, K., and Bibb, J. A. (2016) The emerging role of Cdk5 in cancer. *Trends Cancer* **2,** 606–618
11. Krampitz, G. W., and Norton, J. A. (2014) RET gene mutations (genotype and phenotype) of multiple endocrine neoplasia type 2 and familial medullary thyroid carcinoma. *Cancer* **120,** 1920–1931
12. Donis-Keller, H., Dou, S., Chi, D., Carlson, K. M., Toshima, K., Lairmore, T. C., Howe, J. R., Moley, J. F., Goodfellow, P., and Wells, S. A., Jr. (1993) Mutations in the RET proto-oncogene are associated with MEN 2A and FMTC. *Hum. Mol. Genet.* **2,** 851–856
13. Mulligan, L. M., Kwok, J. B., Healey, C. S., Elsdon, M. J., Eng, C., Gardner, E., Love, D. R., Mole, S. E., Moore, J. K., and Papi, L. (1993) Germ-line mutations of the RET proto-oncogene in multiple endocrine neoplasia type 2A. *Nature* **363,** 458–460
14. Romei, C., Ciampi, R., and Elisei, R. (2016) A comprehensive overview of the role of the RET proto-oncogene in thyroid carcinoma. *Nat. Rev. Endocrinol.* **12,** 192–202
15. Elisei, R., Romei, C., Cosci, B., Agate, L., Bottici, V., Molinaro, E., Sculli, M., Miccoli, P., Basolo, F., Grasso, L., Pacini, F., and Pinchera, A. (2007) RET genetic screening in patients with medullary thyroid cancer and their relatives: experience with 807 individuals at one center. *J. Clin. Endocrinol. Metab.* **92,** 4725–4729
16. Kucherlapati, M. H., Nguyen, A. A., Bronson, R. T., and Kucherlapati, R. S. (2006) Inactivation of conditional Rb by Villin-Cre leads to aggressive tumors outside the gastrointestinal tract. *Cancer Res.* **66,** 3576–3583
17. Akeno, N., Miller, A. L., Ma, X., and Wikenheiser-Brokamp, K. A. (2015) p53 suppresses carcinoma progression by inhibiting mTOR pathway activation. *Oncogene* **34,** 589–599
18. Coxon, A. B., Ward, J. M., Geradts, J., Otterson, G. A., Zajac-Kaye, M., and Kaye, F. J. (1998) RET cooperates with RB/p53 inactivation in a somatic multi-step model for murine thyroid cancer. *Oncogene* **17,** 1625–1628
19. Nilsson, M., and Williams, D. (2016) On the origin of cells and derivation of thyroid cancer: C cell story revisited. *Eur. Thyroid J.* **5,** 79–93
20. Michiels, F. M., Chappuis, S., Caillou, B., Pasini, A., Talbot, M., Monier, R., Lenoir, G. M., Feunteun, J., and Billaud, M. (1997) Development of medullary thyroid carcinoma in transgenic mice expressing the RET protooncogene altered by a multiple endocrine neoplasia type 2A mutation. *Proc. Natl. Acad. Sci. U.S.A.* **94,** 3330–3335
21. Vitale, G., Gaudenzi, G., Circelli, L., Manzoni, M. F., Bassi, A., Fioritti, N., Faggiano, A., Colao, A., NIKE Group (2017) Animal models of medullary thyroid cancer: state of the art and view to the future. *Endocr. Relat. Cancer* **24,** R1–R12
22. Song, H., Yao, E., Lin, C., Gacayan, R., Chen, M. H., and Chuang, P. T. (2012) Functional characterization of pulmonary neuroendocrine cells in lung development, injury, and tumorigenesis. *Proc. Natl. Acad. Sci. U.S.A.* **109,** 17531–17536
23. Kim, E. J., Ables, J. L., Dickel, L. K., Eisch, A. J., and Johnson, J. E. (2011) Ascl1 (Mash1) defines cells with long-term neurogenic potential in subgranular and subventricular zones in adult mouse brain. *PLoS One* **6,** e18472
24. Nagy, A., Gertsenstein, M., Vintersten, K., and Behringer, R. (2003) *Manipulating the Mouse Embryo: A Laboratory Manual*, 3rd Ed., Cold Spring Harbor Laboratory, Cold Spring Harbor, NY
25. Joyner, A. L. (2000) Gene targeting: a practical approach, 2nd Ed., Oxford University Press, Oxford, UK
26. Danielian, P. S., Muccino, D., Rowitch, D. H., Michael, S. K., and McMahon, A. P. (1998) Modification of gene activity in mouse embryos in utero by a tamoxifen-inducible form of Cre recombinase. *Curr. Biol.* **8,** 1323–1326
27. Muzumdar, M. D., Tasic, B., Miyamichi, K., Li, L., and Luo, L. (2007) A global double-fluorescent Cre reporter mouse. *Genesis* **45,** 593–605
28. Soriano, P. (1999) Generalized lacZ expression with the ROSA26 Cre reporter strain. *Nat. Genet.* **21,** 70–71
29. Williams, B. O., Remington, L., Albert, D. M., Mukai, S., Bronson, R. T., and Jacks, T. (1994) Cooperative tumorigenic effects of germline mutations in Rb and p53. *Nat. Genet.* **7,** 480–484

30. Harvey, M., Vogel, H., Lee, E. Y., Bradley, A., and Donehower, L. A. (1995) Mice deficient in both p53 and Rb develop tumors primarily of endocrine origin. *Cancer Res.* **55,** 1146–1151
31. Marino, S., Vooijs, M., van Der Gulden, H., Jonkers, J., and Berns, A. (2000) Induction of medulloblastomas in p53-null mutant mice by somatic inactivation of Rb in the external granular layer cells of the cerebellum. *Genes Dev.* **14,** 994–1004
32. Cerrato, A., De Falco, V., and Santoro, M. (2009) Molecular genetics of medullary thyroid carcinoma: the quest for novel therapeutic targets. *J. Mol. Endocrinol.* **43,** 143–155
33. Robbins, H. L., and Hague, A. (2015) The PI3K/Akt pathway in tumors of endocrine tissues. *Front. Endocrinol.* (*Lausanne*) **6,** 188
34. Groszer, M., Erickson, R., Scripture-Adams, D. D., Lesche, R., Trumpp, A., Zack, J. A., Kornblum, H. I., Liu, X., and Wu, H. (2001) Negative regulation of neural stem/progenitor cell proliferation by the Pten tumor suppressor gene *in vivo*. *Science* **294,** 2186–2189
35. Antico Arciuch, V. G., Russo, M. A., Dima, M., Kang, K. S., Dasrath, F., Liao, X. H., Refetoff, S., Montagna, C., and Di Cristofano, A. (2011) Thyrocyte-specific inactivation of p53 and Pten results in anaplastic thyroid carcinomas faithfully recapitulating human tumors. *Oncotarget* **2,** 1109–1126
36. Champa, D., and Di Cristofano, A. (2015) Modeling anaplastic thyroid carcinoma in the mouse. *Hormones Cancer* **6,** 37–44
37. Viola, D., Valerio, L., Molinaro, E., Agate, L., Bottici, V., Biagini, A., Lorusso, L., Cappagli, V., Pieruzzi, L., Giani, C., Sabini, E., Passannati, P., Puleo, L., Matrone, A., Pontillo-Contillo, B., *et al.* (2016) Treatment of advanced thyroid cancer with targeted therapies: ten years of experience. *Endocr. Relat. Cancer* **23,** R185–R205
38. Spitzweg, C., Morris, J. C., and Bible, K. C. (2016) New drugs for medullary thyroid cancer: new promises? *Endocr. Relat. Cancer* **23,** R287–R297
39. Russo, A., Franchina, T., Ricciardi, G. R., Picone, A., Ferraro, G., Zanghì, M., Toscano, G., Giordano, A., and Adamo, V. (2015) A decade of EGFR inhibition in EGFR-mutated non small cell lung cancer (NSCLC): old successes and future perspectives. *Oncotarget* **6,** 26814–26825
40. Maliszewska, A., Leandro-Garcia, L. J., Castelblanco, E., Macià, A., de Cubas, A., Goméz-López, G., Inglada-Pérez, L., Álvarez-Escolá, C., De la Vega, L., León, R., Gómez-Graña, Á., Landa, I., Cascón, A., Rodríguez-Antona, C., Borrego, S., *et al.* (2013) Differential gene expression of medullary thyroid carcinoma reveals specific markers associated with genetic conditions. *Am. J. Pathol.* **182,** 350–362
41. Pozo, K., Castro-Rivera, E., Tan, C., Plattner, F., Schwach, G., Siegl, V., Meyer, D., Guo, A., Gundara, J., Mettlach, G., Richer, E., Guevara, J. A., Ning, L., Gupta, A., Hao, G., *et al.* (2013) The role of Cdk5 in neuroendocrine thyroid cancer. *Cancer Cell* **24,** 499–511
42. Sastre-Perona, A., and Santisteban, P. (2012) Role of the wnt pathway in thyroid cancer. *Front. Endocrinol.* (*Lausanne*) **3,** 31
43. Jaskula-Sztul, R., Pisarnturakit, P., Landowski, M., Chen, H., and Kunnimalaiyaan, M. (2011) Expression of the active Notch1 decreases MTC tumor growth *in vivo*. *J. Surg. Res.* **171,** 23–27
44. Yu, X. M., Phan, T., Patel, P. N., Jaskula-Sztul, R., and Chen, H. (2013) Chrysin activates Notch1 signaling and suppresses tumor growth of anaplastic thyroid carcinoma *in vitro* and *in vivo*. *Cancer* **119,** 774–781
45. Gujral, T. S., van Veelen, W., Richardson, D. S., Myers, S. M., Meens, J. A., Acton, D. S., Duñach, M., Elliott, B. E., Höppener, J. W., and Mulligan, L. M. (2008) A novel RET kinase-β-catenin signaling pathway contributes to tumorigenesis in thyroid carcinoma. *Cancer Res.* **68,** 1338–1346